

Promotion of Plasma-Induced Deuterium Uptake in Ruthenium Films by Monolayer-Thick Tin Layers

S. C. Wang^{1,2,*}, M. van Kampen³, and T. W. Morgan¹

December 30, 2023

¹DIFFER-Dutch Institute for Fundamental Energy Research, De Zaale 20, 5612 AJ Eindhoven, The Netherlands

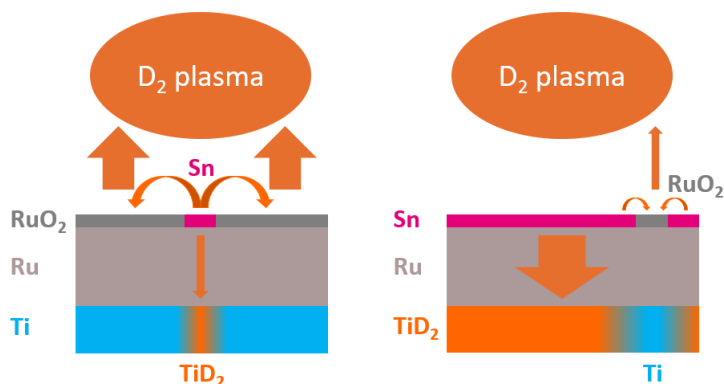
²Department of Applied Physics, Eindhoven University of Technology, P.O. Box 513, 5600MB Eindhoven, The Netherlands

³ASML The Netherlands B.V., P.O. Box 324, 5500AH Veldhoven, The Netherlands

*Author to whom correspondence should be addressed: s.c.wang@diffier.nl

Abstract

Surface impurities can have a significant influence on hydrogen uptake of materials. Examples such as the hydrogen spillover effect demonstrate that even very small surface impurity quantities can lead to order-of-magnitude changes in the total amount of hydrogen taken up by a material. In this work, we report the first experimental demonstration of promoted deuterium uptake in Ru thin films by Sn. Deuterium plasma exposures were carried out for Ru-capped targets covered by Sn up to a few atoms in thickness. After the exposure, the residual Sn content and the deuterium retention were measured to quantify the Sn etching and the deuterium uptake, respectively. By increasing the amount of Sn from zero to one atomic layer on Ru, we found after the exposure that the Sn content stays unchanged while the deuterium uptake rate severely increases with the Sn content by 2–3 orders of magnitude. These results can be understood by simulations using a reaction-diffusion model with multiple surface species and the lateral surface migration of deuterium. By contrast, as the as-deposited Sn content goes above one atomic layer, Sn removal takes place, and the deuterium uptake rate decreases with the as-deposited Sn content. Possible explanations are proposed by considering the interplay between Sn etching and deuterium uptake. In all, this work provides insights into interactions between multiple surface species in relation to plasma-induced hydrogen uptake. By further development,



this could eventually lead to a potential mitigation method to circumvent the promoted hydrogen uptake in Ru-capped films.

Keywords: plasma, hydrogen uptake, deuterium retention, ruthenium, tin, surface coverage, reaction-diffusion model, extreme ultraviolet lithography

1 Introduction

Hydrogen uptake plays a crucial role in a wide variety of research fields where hydrogen atoms have significant impacts on the surface or in the bulk. This uptake can be desirable, such as in hydrogen storage materials, or undesirable, such as in a nuclear fusion reactor, where hydrogen uptake leads to loss of fuel atoms from the fuel cycle and hydrogen-induced embrittlement in pipelines. These results all show the importance of hydrogen uptake and the need for a detailed investigation of the influential factors.

Hydrogen uptake can be influenced by a trace amount of an additional substance on the absorbing material. Upon hydrogen gas exposure, Pt nanoparticles with sizes of 3–9 nm on a carbon nanotube (CNT) support can cause an increase in the hydrogen storage capacity by nearly 40 times [1]. This drastic enhancement is attributed to the so-called spillover effect: the Pt catalyst facilitates dissociation of hydrogen molecules to generate hydrogen atoms, which spill over the supporting CNTs due to strong interactions between Pt nanoparticles and the CNT support [2]. Surface modifications can also affect hydrogen uptake in materials irradiated by hydrogen ions. A recent study shows that a submonolayer of oxygen on the W surface decreases the ion-induced deuterium uptake because oxygen occupies the surface sites for deuterium adsorption [3]. This indicates that a tiny amount of surface impurities should not be easily ignored because they can have a significant influence on the hydrogen uptake in the absorbing material.

It has been extensively studied that hydrogen plasmas or radicals can be used as a cleaning agent to remove the Sn deposition by forming volatile species

SnH_4 [4, 5]. However, van Herpen *et al.* reported that as the Sn layer deposited on Ru is reduced by hydrogen radicals to a few nm thick, the removal rate decreases to almost zero and delamination of the Ru film starts to occur [4]. The ceased Sn removal is attributed to SnH_4 decomposition and subsequent Sn redeposition on Ru due to strong interactions between Sn and Ru, as experimentally demonstrated in [6, 7]. On the other hand, delamination of the Ru film is commonly considered as a result of strong hydrogen uptake, leading to blister formation and film ruptures [8, 9]. This could indicate enhanced hydrogen uptake in the Ru film in the presence of a small amount of Sn debris. Recent density functional theory (DFT) studies also suggest that one atomic layer of Sn on Ru induces charge transfer and effectively lowers the hydrogen absorption barrier to the Ru subsurface [10, 11]. Nevertheless, this hydrogen uptake promotion has never been studied experimentally, possibly due to the difficulty with keeping the Ru film from cracking and analyzing the hydrogen uptake quantitatively [4].

In this work, we demonstrate for the first time the promotion of hydrogen uptake in Ru films in the presence of Sn. For quantitative analysis of the hydrogen uptake, we performed ex-situ experiments which include the following steps:

1. Ru and Ti films were deposited on a Si wafer to produce the Ru-capped target.
2. A spatially varying layer of Sn of thickness was deposited on the Ru-capped target.
3. Sn layer thickness on the target was quantified using ion beam analysis.
4. The Sn-coated target was loaded with deuterium by deuterium plasma exposure.
5. The residual Sn layer thickness and deuterium retention in the target were quantified using ion beam analysis.

The steps 1–5 were repeated for multiple targets to study the influence of the Sn content, the plasma fluence, and the ion energy. These targets were stored under ambient conditions between each step. The experimental results indicate two regimes for the Sn content below and above one atomic layer. For a single atomic layer of Sn, we found a termination of Sn removal and accelerated deuterium uptake as van Herpen *et al.* discovered in [4]. A reaction-diffusion model is applied to understand the deuterium uptake enhancement and to determine the barriers for critical processes. In the other regime for more than one atomic layer of Sn, Sn removal and deuterium uptake turn out to be quite different from those for an atomic layer of Sn. This will also be discussed and possible explanations will be proposed.



Figure 1: Schematic of the film stack of the target before Sn deposition.

2 Materials and Methods

2.1 Target Preparation

2.1.1 Ru-Capped Ti Targets

The targets we used in this work were Sn-covered Ru and Ti films on Si (100) substrates with a 25.4 mm (1 in.) diameter and flat orientation. The target was prepared in two steps: first, the Ru and Ti films with nominal thicknesses of 40 and 30 nm, respectively, were prepared by magnetron sputtering at Philips Engineering Solutions. After the deposition, RuO_2 was formed on the surface upon exposure to air, and the film stack is shown in Fig. 1. Second, the Sn layer was deposited in an experimental setup at Advanced Semiconductor Materials Lithography (ASML), which will be described in the next section. The detailed characteristics of the Ru and Ti films have been described in [12] and a short summary is given here. This target design deploys the Ti layer as a deuterium absorption layer protected by the Ru capping layer against oxidation. When the target is exposed to a deuterium plasma, deuterium has to permeate the Ru layer before absorption occurs at the Ti layer. In this way, the deuterium retention in the Ti layer can be measured to quantify the deuterium uptake rate of the Ru capping layer. The Ru layer was a polycrystalline film with a dominant (0001) orientation. The areal densities of the Ru and Ti films were $(2.9 \pm 0.23) \times 10^{21}$ and $(1.75 \pm 0.14) \times 10^{21}$ atoms/m², respectively, according to Rutherford backscattering spectroscopy (RBS) measurements as described in detail in [12]. If we assume a Ru density of 12.2 g/cm³ and a Ti density of 4.54 g/cm³, the Ru and Ti films had thicknesses of 39.9 ± 3.2 and 30.6 ± 2.4 nm, respectively. Based on these experimental results, we assume a pure Ru(0001) surface and define 1 monolayer (ML) as an overlayer with the atomic density of the Ru surface, which equals 1.74×10^{19} atoms/m² according to the measured areal density of the Ru film. The RuO_2 layer on the surface was approximately 1 ML in thickness as confirmed in our previous work in [12].

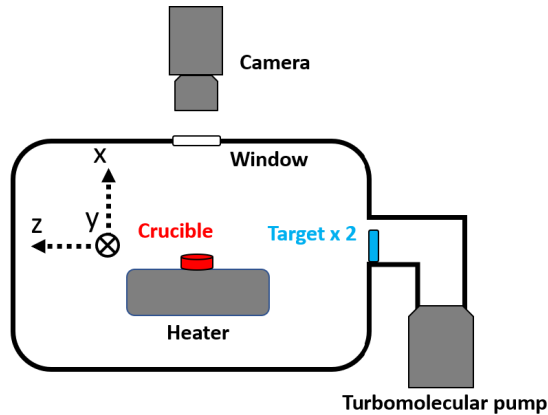
2.1.2 Sn Deposition and Quantification

An ASML’s experimental setup called Diablo was used for physical vapor deposition of Sn on Ru-capped targets via thermal evaporation. A schematic of Diablo is shown in Fig. 2(a). It consists of a cylindrical vacuum vessel with a 200 mm diameter (in the xy plane) and a 300 mm length (on the z-axis). The setup was equipped with a Pfeiffer HiPace 80 turbo pump and a tectra Boralectric heater. Our deposition process placed two Ru-capped Si targets and a Sn-filled Mo crucible in Diablo. The Ru-coated sides of the targets face the crucible as shown in Fig 2(a). The two targets were placed 150 mm away from the crucible, and the distance between them was 5 mm. The Mo crucible was prewetted with 5 g of Sn (Cleanpart GmbH, purity 99.9%) and placed on the ceramic surface of the heater. After the setup was pumped to the pressure of 10^{-6} mbar, Sn was evaporated by the heater into the vacuum chamber and deposited on the targets. The corresponding temperature of the Sn crucible was 880°C , based on thermocouple measurements, and the pressure was 10^{-4} mbar during Sn evaporation. We set the deposition time in the range of 120 to 1200 s based on the desired content of Sn. The content of deposited Sn was less than 1.5 ML, which corresponds to 2.61×10^{19} atoms/ m^2 when we use the Ru substrate as the reference layer. We assume β -tin in our experiment because it is stable at room temperature. Based on earlier experimental and theoretical studies, we assume that for the Sn content less than 0.67 ML, a two-dimensional layer of Sn is formed on the Ru surface [13, 14, 15, 11]. More than 0.67 ML of Sn leads to three-dimensional (3D) growth on the first atomic layer of Sn.

It is important to note that in Diablo, the two Ru targets sat close to the pump duct and did not receive a uniform sublimation flow from the Sn crucible. Therefore, we typically had a one-dimensional gradient of the Sn content on both Ru-capped targets as shown in Fig. 3. We assume in each deposition process, the areal density of Sn deposited on both targets had the same spatial distribution. This gradient made it convenient to scan the Sn content within a single target. Together with the capability of detecting local concentrations using RBS and elastic recoil detection (ERD), we were able to investigate the correlation between the Sn and D contents of the target exposed to a deuterium plasma.

2.2 Deuterium Plasma Exposures

The work on deuterium plasmas was performed using the nano-PSI device at DIFFER. The details of nano-PSI can be found in [16, 12] but a short description is given here. Nano-PSI is an experimental setup at DIFFER to study plasma surface interactions (PSI) [17]. Plasmas in nano-PSI are generated by a cascaded arc source [18, 19]. During operation of the plasma source, the gas flow into the source was 1.5 slm, the vessel pressure was 45 Pa, the cathode current was set to 40 A, and the characteristic cathode voltage was 130 V for deuterium plasmas. At this setting, the electron temperature was 0.21 ± 0.024 eV, the ion flux $(4.2 \pm 0.47) \times 10^{19}$ $\text{m}^{-2}\text{s}^{-1}$, the radical flux $(2.3 \pm 0.32) \times 10^{22}$ $\text{m}^{-2}\text{s}^{-1}$, and the FWHM



(a)

Figure 2: Schematic of ASML’s Diablo in Veldhoven. In this work, Diablo serves as a vacuum setup for physical vapor deposition of Sn on two Ru-capped Si targets. Their surface normals and the flats point toward the $+z$ and $-x$ directions, respectively. Both targets have the same x - and z -coordinates in the setup, and they are placed at different locations on the y -axis.

of the plasma beam was 67.2 ± 2.6 mm, according to measurement results using a double Langmuir probe described in [16]. A target was mounted on a water-cooled target holder, and the target surface was 100 mm away from the nozzle of the plasma source. The target had a circular area with a diameter of 18 mm, which is much smaller than the plasma diameter, such that the loading of the surface can be considered uniform. The energy of ions arriving at the target was expected to be 1 and 20 eV when the target was floating and biased to -20 V, respectively [12].

2.3 Ion Beam Analysis

We used RBS to determine the Sn content on the target before and after plasma exposure, and we used ERD to measure the amount of deuterium in the target after plasma exposure. The details of the measurement techniques are described in [12], and here we give a brief summary as well as the measurement strategy for each target. The experiments were carried out at the DIFFER ion beam facility (IBF), where we used a $^4\text{He}^+$ beam at 2.4 MeV, and a fraction of the incident beam was backscattered by a chopper for relative ion dose control [20]. The irradiation area on the target was 1×1 mm² for both RBS and ERD. As mentioned in Sec. 2.1.2, there was a gradient in the Sn content on each target after the deposition process in Diablo. To investigate the influence of the Sn content on the deuterium uptake, we performed IBF measurements at multiple locations along the x -axis of each target, which was the direction of the gradient

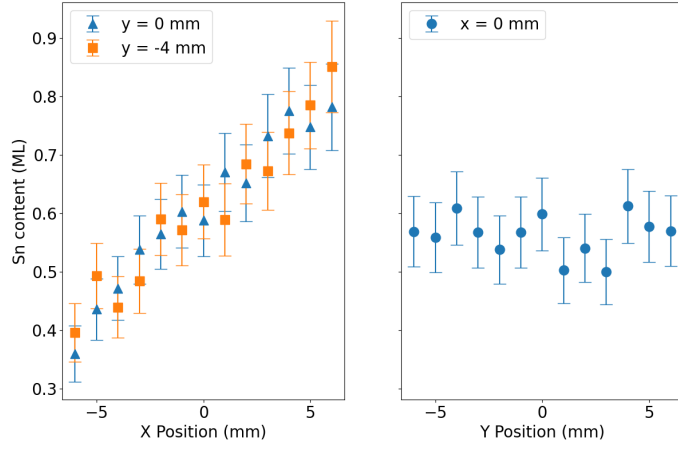
as shown in Fig. 3(a). These locations can be the same before and after the plasma exposure for each target. However, surface impurities such as carbon can be introduced to the target surface by ion beam irradiation in the presence of hydrocarbon background gas [21]. Carbon on the surface can act as a sacrificial layer and lower the deuterium retention induced by the plasma exposure [22]. To minimize the influence of impurities on the deuterium uptake, before the plasma exposure, we performed RBS measurements to quantify the Sn content at five locations 4 mm away from the x-axis as indicated by the triangles in Fig. 3. After the plasma exposure, we performed RBS and ERD measurements at five other locations on the x-axis as indicated by the squares in the same figure. These five squares have the same x-coordinates, respectively, as the five triangles. Since there was no gradient in the Sn content along the y-axis according to the measurements shown in Fig. 3(a), we can assume the same Sn content at locations with the same x-coordinate. As a result, we can determine the Sn content before and after plasma exposure as well as the plasma-induced deuterium retention at multiple locations of each target.

In the RBS configuration, we set the incident angle $\alpha = 4^\circ$ and the scattering angle of 170° in Cornell geometry. A Si target coated with $(6.5 \pm 0.52) \times 10^{21}$ atoms/m² of Pt was used as the RBS reference target and we obtained its RBS spectrum in the same configuration as the Sn-deposited Ru-capped targets. Typical RBS spectra of Ru-capped targets before and after Sn deposition are shown in Fig. 4. Compared to the spectrum of the as-deposited Ru-capped target, the spectrum of Sn-covered target has an extra peak in the 2072–2122 keV range, which corresponds to the Sn deposited on the Ru surface, according to analysis using SIMNRA [23]. The Sn areal density $(Nt)_x$ can be obtained using the equation below [20],

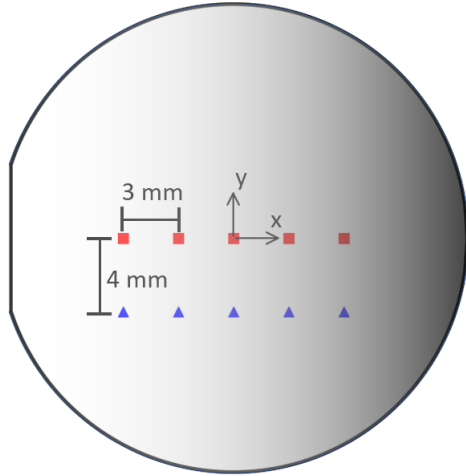
$$(Nt)_x = \frac{A_x \sigma_r Q_r}{A_r \sigma_x Q_x} (Nt)_r \quad (1)$$

where $(Nt)_r$ is the Pt areal density in the RBS reference target. A_i , σ_i , and Q_i ($i = x, r$) refer to the spectral area of the element of interest, the average RBS cross section, and the ion dose on the target, respectively. The subscripts x and r refer to Sn on the Sn-covered target and Pt on the RBS reference target, respectively. For the RBS reference target with $(Nt)_r$ of 6.5×10^{21} atoms/m², A_r is obtained using the Pt peak in its RBS spectrum, and the average RBS cross section of $^4\text{He}^+$ in Pt (σ_r) can be determined using SIMNRA. For the Sn-covered target, A_x is calculated using the Sn peak in the RBS spectrum as shown in Fig. 4, and σ_x is obtained using SIMNRA by assuming the energy loss of $^4\text{He}^+$ in Sn is negligible since we have only MLs of Sn. By setting $Q_x = Q_r$ using the chopper in the measurement, we can determine the Sn areal density using Eq. 1.

In the ERD configuration, we set the incident angle $\alpha = 75^\circ$ and the recoil angle of 30° in IBM 1 geometry [23]. A Mylar foil of 1.26×10^{24} atoms/m² (13.2 μm in thickness) was placed in front of the ERD detector to stop the scattered ^4He at the recoil angle, such that only signals of recoil hydrogen and deuterium particles were received at the ERD detector. Similar to our RBS measurements,



(a)



(b)

Figure 3: (a) Sn contents measured by RBS at various locations on the Ru-capped target. The origin refers to the center of the target, and the x- and y-axes are defined in Fig. 3(b). The surface normal and orientation flat point toward the +z and -x direction, respectively. Note that when the target sits in Diablo, the x- and z-axes of the target are the same as those of Diablo, as defined in Fig. 2. The left plot shows a similar one-dimensional gradient along the x-axis for different y-coordinates, which originates from the orientation of the target during the deposition process. The right plot shows a similar Sn content at the locations with the same x-coordinate. (b) Measurement locations on the target for ion beam analysis, as described in detail in the text. The irradiation area on the target was $1 \times 1 \text{ mm}^2$ for both RBS and ERD. The grayscale gradient on the wafer illustrates the gradient of the Sn thickness along the x-axis. The dark area has a thicker Sn layer than the light area according to the measured distribution shown in (a).

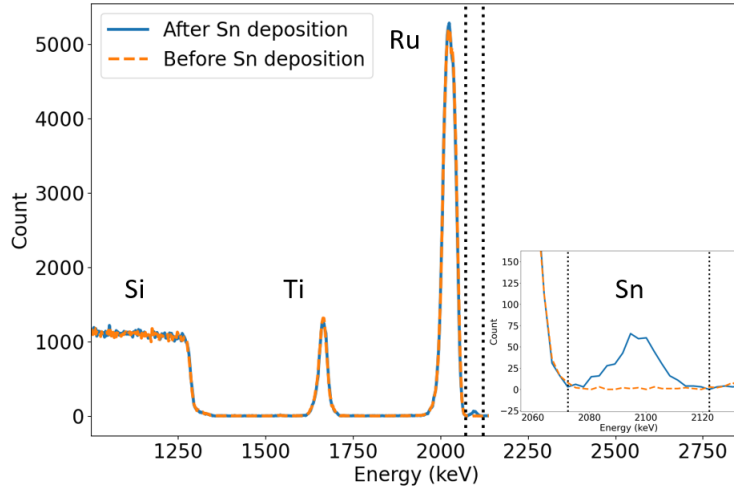


Figure 4: Typical RBS spectra of the target before and after Sn deposition. The dashed and solid lines refer to RBS spectra for the Ru-capped target before and after a Sn deposition, respectively. The Sn peak after the Sn deposition appears in the region between the dotted lines as shown in the inset. We use the spectral area of the Sn peak to determine the Sn content.

the ERD measurements involved an ERD reference target with a predetermined deuterium content [12]. The spectrum of the ERD reference target was obtained in the same configuration as those of plasma-exposed Sn-covered targets. This way the deuterium areal density in the Sn-covered target could be determined based on the corresponding spectral area relative to that of the ERD reference target, as described in [12].

3 Experimental Results

3.1 Saturation of Ti with Deuterium

After plasma exposure, deuterium was retained in the Ti layer of the target. We can use this retention to quantify the deuterium uptake induced by the plasma as long as the Ti layer is not saturated by deuterium under our experimental conditions. We examined this criterion by performing a plasma fluence scan for the target which contains the Sn content of interest, approximately 0.6 ML. The ion energy (E_{ion}) was 1 eV during the plasma exposures and the deuterium retention in these targets was measured using ERD as shown in Fig. 5. For targets without deposited Sn, our previous work shows that the retention in the target linearly increased with the exposure time (t_{exp}) up to 1080 s, and the uptake rate was 2×10^{17} atoms/m²/s for the same plasma setting as this work [12]. In contrast, for targets with approximately 0.6 ML of Sn, the deu-

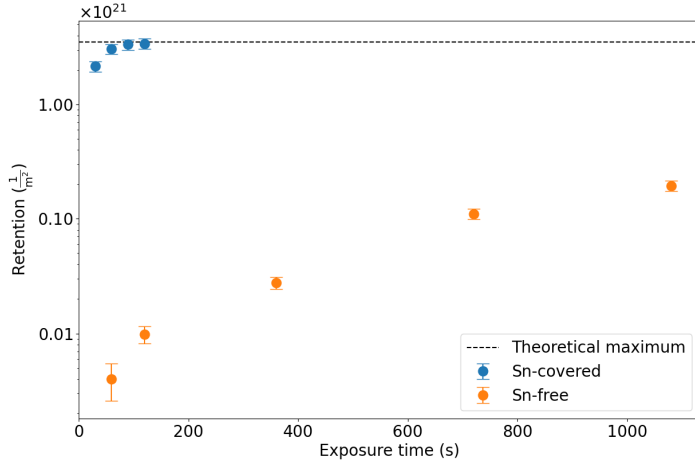


Figure 5: Deuterium retention in the Sn-covered and Sn-free targets exposed to the deuterium plasma at an ion energy of 1 eV. RBS measurements give the Sn content on the Sn-covered target before the plasma exposure. There was 0.58 ± 0.07 ML of Sn on the targets exposed for 30 and 60 s, and 0.61 ± 0.07 ML of Sn on the targets exposed for 90 and 120 s. After the exposures, the deuterium retention was measured using ERD.

terium retention rose to $(2.15 \pm 0.21) \times 10^{21}$ atoms/m² after 30 s of exposure and almost reached saturation within 120 s as shown in Fig. 5. This clearly demonstrates a great influence of this 0.6 ML of Sn on the deuterium uptake rate, given that the average deuterium uptake rate for the first 30 s was $(7.16 \pm 0.72) \times 10^{19}$ atoms/m²/s, which is more than 300 times higher than that without Sn. At 120 s, the deuterium retention reaches $(3.4 \pm 0.34) \times 10^{21}$ atoms/m², which can be explained by deuteration of almost the entire Ti layer to form TiD₂ since we had $(1.75 \pm 0.14) \times 10^{21}$ atoms/m² of Ti in the target [24]. Therefore, in this work, we chose the plasma parameters for exposures so that the deuterium retention was kept below the theoretical saturation level at 3.5×10^{21} atoms/m² (defined later in Sec. 4 as $n_{trap,max}$) and can be used for quantification of the deuterium uptake rate. It is also worthwhile to note that in this fluence scan, we did not observe cracks or ruptures of blisters on the target, which indicates that deuterium implanted by the plasma stayed in the target without being released via opening of the capping layer. This is also an important criterion for our experiments in addition to the deuterium retention being less than 3.5×10^{21} atoms/m². These two criteria are applied to all the experiments presented in this work.

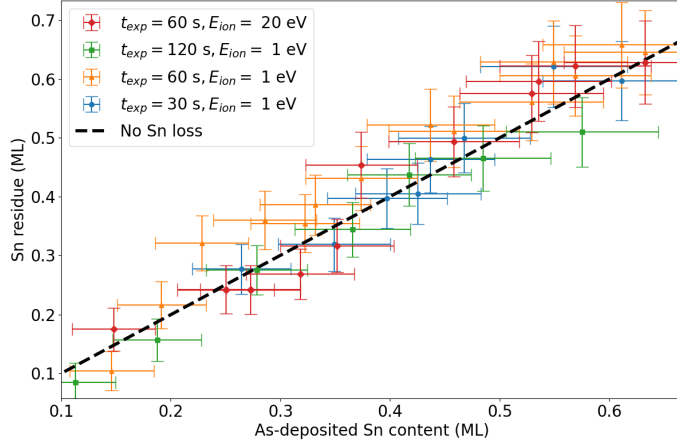
3.2 Influence of Sn

To investigate how Sn affects the deuterium uptake, we varied the as-deposited Sn content on the target as described in Sec. 2.1.2, and measured the residual Sn content and the deuterium retention after a plasma exposure as shown in Fig. 6. Focusing first on Sn less than one atomic layer, we scanned the as-deposited Sn content from 0 to 0.67 ML, which was repeated four times for plasma exposures with different plasma parameters. A fluence scan by varying the exposure time (t_{exp}) was performed at an ion energy (E_{ion}) of 1 eV and a series of 60 s exposures was performed at an ion energy of 20 eV. During all the plasma exposures, the gas flow was 1.5 slm and the pressure was 45 Pa.

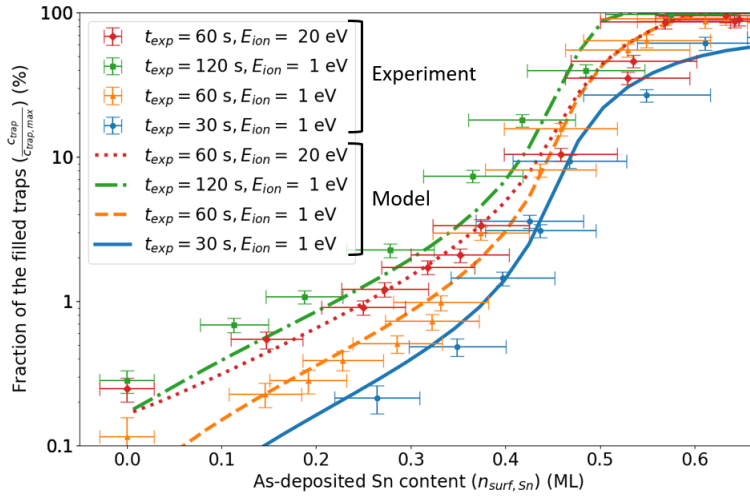
We also investigated the residual Sn content after the exposure, since it has been reported that Sn etching occurs in the presence of hydrogen plasma [25, 26, 27]. However, given the error of the RBS measurement, we cannot prove a correlation between the etched Sn content and the plasma exposure time as shown in in Fig. 6(a). There appears to be no loss of Sn on the target after all the exposures, which means Sn effectively stayed at the Ru surface of the target throughout the plasma exposure. Similar phenomena have been reported for Sn etching from Ru surfaces using hydrogen radicals [4, 7]. Further experiments with high accuracy are needed to verify our preliminary conclusion regarding the stagnant layer of Sn on Ru. On the other hand, as already indicated in Sec. 3.1, we observe the deuterium retention drastically increases with the as-deposited Sn content as shown in the logarithmic plot in Fig. 6(b). These results, for the first time, exhibit the influence of Sn on plasma-induced deuterium uptake in Ru films as predicted in a recent study based on DFT [10].

The plasma parameters also have effects on the deuterium uptake rate. At an ion energy of 1 eV, the deuterium retention increases with fluence regardless of the as-deposited Sn content. On the other hand, the deuterium uptake rate appears to increase with the ion energy only when the as-deposited Sn content is less than 0.5 ML. Besides qualitative comparison, these results can help us to gain understanding with a reaction-diffusion model and identify relevant processes to the deuterium uptake. The details of the model will be discussed later in Sec. 4.

To gain a greater understanding of the influence of Sn, we also performed experiments for more than one atomic layer of the as-deposited Sn. We varied the as-deposited Sn content from 0.67 to 1.5 ML, and the target was exposed to the deuterium plasma for 30 and 60 s at an ion energy of 1 eV. As shown in Fig. 7, both the residual Sn content and the deuterium retention have totally different behaviors from those for less than one atomic layer of the as-deposited Sn. First, the residual Sn content is less than the as-deposited Sn content, which is expected to occur as a result of plasma-induced Sn etching [6]. This process of Sn loss probably lasts for less time than 30 s given no significant difference in the residual Sn content between the 30 and 60 s exposures. Second, contrary to the drastic acceleration for less than one atomic layer of Sn, the deuterium uptake *decreases* with the as-deposited Sn content for the 30 s exposures. Note that we lose Sn within this 30 s based on the measured residual Sn content,



(a) The residual Sn content on the Sn-covered target.



(b) The deuterium retention in the Sn-covered target.

Figure 6: Results of ion beam analysis of the Sn-covered target exposed to the deuterium plasma. The Sn content before plasma exposure ranged from 0 to 0.67 ML, and the exposures were performed with four different plasma parameters. Note that the residual Sn content is plotted with a linear scale, whereas the deuterium retention is plotted with a logarithmic scale. (a) Residual Sn content is expressed in ML. The dashed line refers to equal amounts of the residual and as-deposited Sn, which indicates effectively no Sn etching. (b) Measured and calculated deuterium retention in the target. The calculation is performed using the model described in Sec. 4 with the fixed parameters in Tab. 1 and 2, and the best-fit values of the free parameters in Tab. 3. The deuterium retention is expressed in the fraction of the filled traps in the Ti layer, which becomes fully filled for the deuterium retention of 3.5×10^{21} atoms/m².

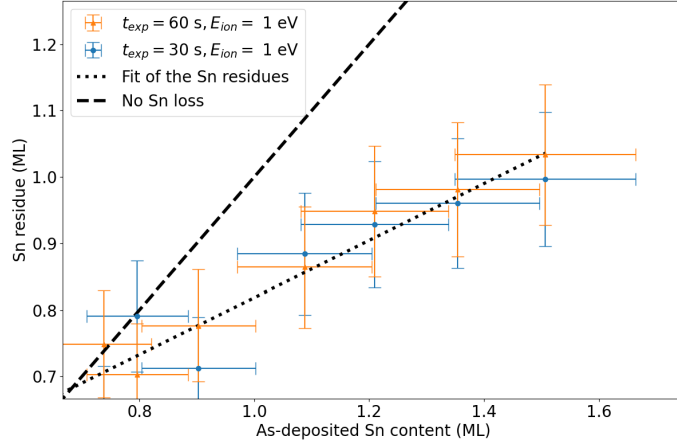
possibly leading to a time-evolving influence of Sn during this period. As we increase the exposure time from 30 to 60 s, the deuterium retention increases but becomes independent of the as-deposited Sn content. This indicates that from 30 to 60 s, the amount of retained deuterium increases with the as-deposited Sn content, which is the opposite of the trend we observe for exposures from 0 to 30 s. The change of the deuterium retention will be used for estimation of the uptake rate to investigate the interactions between deuterium, Sn, and Ru, as discussed later in Sec. 5.

4 Model

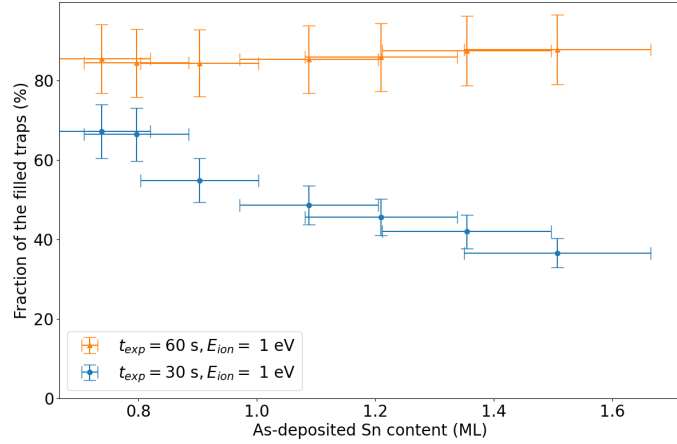
A reaction-diffusion model has been built to understand the influence of Sn on the deuterium uptake in Ru films. This is an extension of our previous model to study plasma-induced deuterium uptake in Ru films in absence of Sn, as described in detail in [12]. In that work, deuterium is implanted into a Ru-capped target covered with a ML of Ru oxide under plasma exposure. Our previous model incorporates surface processes related to the deuterium uptake and fits the measured deuterium retention. According to the model, the deuterium uptake occurs only after the Ru oxide surface is removed by the plasma because hydrogen desorbs from Ru oxide at a lower temperature than metallic Ru [28]. After the onset of the deuterium uptake, the uptake rate is governed by the deuterium surface coverage and the absorption barrier at the Ru surface. These surface parameters are expected to be important also for Sn-deposited Ru films since a different absorption barrier for Sn than Ru is predicted by the DFT work in [10, 11]. Therefore, in this work, we leverage the parameters for metallic Ru from [12], and extend our previous model by adding parameters for RuO₂ and Sn as well as relevant surface processes.

It is very important to note that the extended model only deals with less than one atomic layer of Sn deposited on Ru. In this situation, we can simplify the interactions between Sn, Ru, and deuterium by making the following assumptions for the model:

1. For less than 0.67 ML of the as-deposited Sn, the Ru surface is wetted up to a single layer of Sn atoms without 3D islands. This is supported by the experimental and computational work in [13, 14, 15] and [11], respectively.
2. The target is exposed to air after Sn deposition. As a result, before the plasma exposure, the Ru bulk is partially covered by an atomic layer of tin oxide. The rest of the surface area is covered by a ML of RuO₂.
3. The time for reducing an atomic layer of tin oxide using the deuterium plasma is much shorter than the exposure time, which ranges from 30 to 120 s. This assumption holds based on a reduction rate of 40 nm/min for SnO₂ achieved using hydrogen radicals generated by hot tungsten wires [29]. This reduction rate is equivalent to 1 ML/s in respect to our definition of ML if we assume a SnO₂ density of 6.95 g/cm³. It has been also



(a) The residual Sn content on the Sn-covered target.



(b) The deuterium retention in the Sn-covered target.

Figure 7: Results of ion beam analysis of the Sn-covered target exposed to the deuterium plasma. The Sn content before the plasma exposure was above 0.67 ML, and the exposures were performed for 30 and 60 s at an ion energy of 1 eV. (a) Residual Sn content is expressed in ML. The dashed line refers to equal amounts of the residual and as-deposited Sn, and the dotted line refers to a linear fit of the amount of the residual Sn, as discussed in detail in Sec. 5.2. (b) Deuterium retention is expressed in the fraction of the filled traps in the Ti layer.

demonstrated that approximately one ML of SnO₂ can be reduced by hydrogen plasma exposure in less than 14 s [30]. We therefore neglect Sn oxide in the model and assume we start with a mixed Sn and RuO₂ surface.

4. No Sn etching occurs upon deuterium plasma exposure, which means the residual Sn content equals that of the as-deposited Sn, based on the experimental result shown in Fig. 6. This result appears to be counterintuitive given that Sn removal can be achieved using a hydrogen plasma due to formation of volatile SnH₄ [27]. On the other hand, experiments in [4, 6, 7] also show that Sn etching can be strongly hindered for a thin Sn layer on Ru surface. Therefore, we can make the valid assumption that during the plasma exposure, this single layer of Sn does not leave the Ru surface so the Sn content stays unchanged.

These assumptions lead to three possible surface compositions in the model. The target surface starts with less than an atomic layer of Sn and a submonolayer of RuO₂. The Sn surface coverage θ_{Sn} is an important constant controlled by the deposition process on Diablo. For any given θ_{Sn} , $\theta_{Ru} = 0$ and $\theta_{RuO_2} = 1 - \theta_{Sn}$ at the start of the plasma exposure, where θ_{Ru} and θ_{RuO_2} refer to the Ru and RuO₂ surface coverages respectively. During the plasma exposure, the Sn content remains constant while the Ru surface content emerges as a result of the reduction of the RuO₂ surface, which implies that θ_{Ru} increases, θ_{RuO_2} decreases, and the relationship $\theta_{Ru} + \theta_{RuO_2} = 1 - \theta_{Sn}$ always holds. The oxide removal rate depends on the ion flux and the ion energy as shown in our previous work [12]. Owing to different energy barriers for deuterium at Sn, RuO₂, and Ru surfaces, we differentiate the deuterium content and uptake rates associated with the three surfaces. The model calculates the time evolution of one Ru concentration at the surface and eight deuterium concentrations at different locations, as described below,

1. The areal density of metallic Ru at the surface (n_{Ru}) in m⁻²
2. The deuterium areal density at the surface covered by RuO₂ (n_{surf,RuO_2}) in m⁻²
3. The deuterium areal density at the surface covered by Sn ($n_{surf,Sn}$) in m⁻²
4. The deuterium areal density at the metallic Ru surface ($n_{surf,Ru}$) in m⁻²
5. The deuterium concentration at the subsurface underneath the Sn-covered surface ($c_{sub,Sn}$) in m⁻³
6. The deuterium concentration at the subsurface underneath the metallic Ru surface ($c_{sub,Ru}$) in m⁻³
7. The concentration of mobile deuterium in the Ti layer (c_{bulk}) in m⁻³
8. The concentration of trapped deuterium in the Ti layer (c_{trap}) in m⁻³

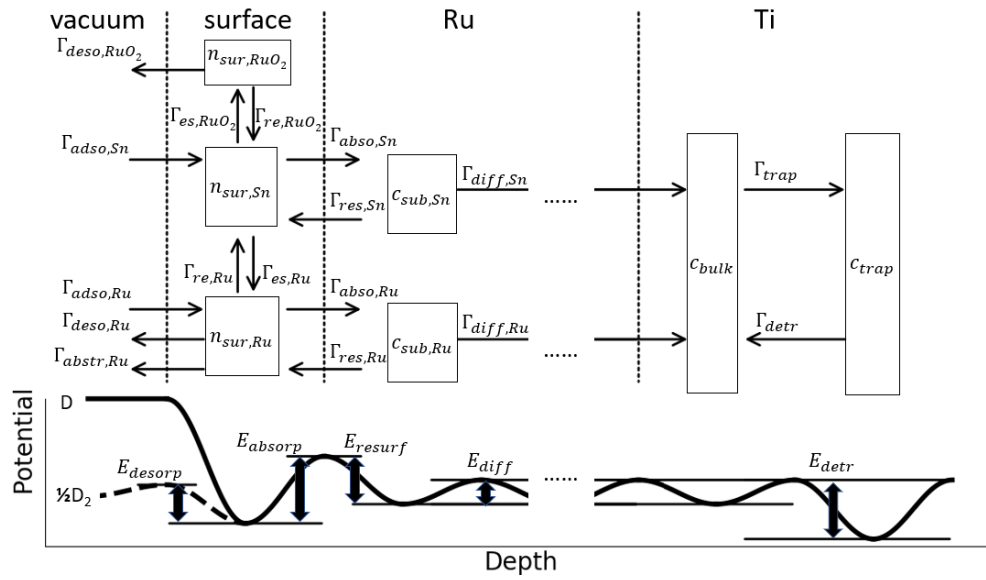


Figure 8: Potential diagram to describe the energy barriers which deuterium atoms need to overcome when migrating from the Ru surface to the bulk or the vacuum. Time evolution of the deuterium concentrations is described by Eq. 2 and the relevant deuterium fluxes indicated by single-headed arrows are defined in Eq. 3.

These concentrations are relevant to the main processes in this model to correlate the deuterium fluxes from the plasma to the deuterium retention (c_{trap}). These processes can be associated with depth-wise or lateral surface transport of deuterium in the system as depicted in Figure 8. The depth-wise transport through the layers are described in detail in [12], and a brief outline is given here. All the concentrations start with zero in the initial condition. During the plasma exposure, deuterium coming from the plasma first sticks to the surface given weak desorption and abstraction at room temperature, leading to a high surface concentration $c_{surf,i}$ where $i = \text{Sn, Ru}$. Next, deuterium penetration of the surface causes a high deuterium concentration at the subsurface $c_{sub,i}$ (where $i = \text{Sn, Ru}$), followed by deuterium diffusion from the subsurface to the Ti layer with a deuterium concentration c_{bulk} . These deuterium atoms become trapped in the Ti layer when c_{trap} is below the maximum concentration of trapped deuterium. Similar processes occur both for Ru and Sn surfaces with different penetration fluxes. Note that this model excludes deuterium concentrations below the RuO_2 surface and the associated deuterium uptake is neglected due to a high barrier for hydrogen penetration of a RuO_2 surface [31]. It is also worthwhile to note that this model excludes direct implantation by deuterium ions at energies of 1 and 20 eV, which was treated in the same way in our previous model [12].

In addition to the depth-wise transport described above, this model includes processes for the lateral surface transport of deuterium at the surface with three possible compositions. Deuterium on the Sn surface can “escape” to the RuO_2 or Ru surface as indicated by $\Gamma_{es,j}$ (where $j = \text{RuO}_2, \text{Ru}$) in Figure 8. These escape fluxes are energetically possible given that hydrogen is 0.75 – 1.33 eV higher in energy in the presence of Sn than without Sn on Ru, based on a recent DFT study [11]. Deuterium can quickly spread out on the Ru surface after the escape since the deuterium diffusion coefficient is $4.2 \times 10^{-11} \text{ m}^2/\text{s}$ for the Ru surface [32], approximately 100 times that for the Ru bulk [33]. We assume $\Gamma_{es,j}$ is determined by the associated deuterium surface coverages and an activation barrier E_{es} , which deuterium needs to overcome for the state transition. This model also includes the complementary deuterium fluxes from RuO_2 or Ru to Sn as indicated by $\Gamma_{re,j}$ (where $j = \text{RuO}_2, \text{Ru}$) in Figure 8. However, these “return” fluxes are expected to be much lower than $\Gamma_{es,j}$ because a large barrier (E_{re}) needs to be overcome to reach the high-energy state of deuterium on Sn [11]. Note that we exclude the deuterium flux from the Ru to RuO_2 surface in the model because it is energetically more favorable for hydrogen atoms to stay adsorbed on Ru than RuO_2 [34, 31]. The deuterium flux from the RuO_2 to Ru surface is also excluded in the model due to strong deuterium desorption from the RuO_2 surface [28] and scarcity of empty sites on the Ru surface [12].

Depth-wise and lateral deuterium fluxes constitute the model for calculation of nine concentrations in the system. Based on Ru oxide removal and conservation of deuterium atoms, we have the following differential equations

$$\begin{aligned}
\frac{dn_{Ru}}{dt} &= \Gamma_{removal} \\
\frac{dn_{surf,RuO_2}}{dt} &= \Gamma_{es,RuO_2} - \Gamma_{re,RuO_2} - \Gamma_{desorp,RuO_2} \\
\frac{dn_{surf,Sn}}{dt} &= -\Gamma_{es,RuO_2} + \Gamma_{re,RuO_2} - \Gamma_{es,Ru} + \Gamma_{re,Ru} + \\
&\quad \Gamma_{adsorp,Sn} - \Gamma_{absorp,Sn} + \Gamma_{resurf,Sn} \\
\frac{dn_{surf,Ru}}{dt} &= \Gamma_{es,Ru} - \Gamma_{re,Ru} + \Gamma_{adsorp,Ru} - \Gamma_{abstr,Ru} \\
&\quad - \Gamma_{desorp,Ru} - \Gamma_{absorp,Ru} + \Gamma_{resurf,Ru} \\
\lambda_{Ru} \frac{dc_{sub,Sn}}{dt} &= \Gamma_{absorp,Sn} - \Gamma_{resurf,Sn} - \Gamma_{diff,Sn} \\
\lambda_{Ru} \frac{dc_{sub,Ru}}{dt} &= \Gamma_{absorp,Ru} - \Gamma_{resurf,Ru} - \Gamma_{diff,Ru} \\
d_{Ti} \frac{dc_{bulk}}{dt} &= \Gamma_{diff,Sn} + \Gamma_{diff,Ru} - \Gamma_{trap} + \Gamma_{detr} \\
d_{Ti} \frac{dc_{trap}}{dt} &= \Gamma_{trap} - \Gamma_{detr}
\end{aligned} \tag{2}$$

where the fluxes are defined as

$$\begin{aligned}
\Gamma_{removal} &= \Gamma_{ion}\xi(1 - \theta_{Sn} - \theta_{Ru} - \theta_{D,RuO_2}) \\
\Gamma_{es,RuO_2} &= k_{es}n_{surf,Sn}(1 - \theta_{Sn} - \theta_{Ru} - \theta_{D,RuO_2}) \\
\Gamma_{es,Ru} &= k_{es}n_{surf,Sn}(\theta_{Ru} - \theta_{D,Ru}) \\
\Gamma_{re,RuO_2} &= k_{re}n_{surf,RuO_2}(\theta_{Sn} - \theta_{D,Sn}) \\
\Gamma_{re,Ru} &= k_{re}n_{surf,Ru}(\theta_{Sn} - \theta_{D,Sn}) \\
\Gamma_{adsorp,Sn} &= \Gamma_{atom}(\theta_{Sn} - \theta_{D,Sn}) \\
\Gamma_{adsorp,Ru} &= \Gamma_{atom}\sigma_{adsorp,Ru}(n_{Ru} - n_{surf,Ru}) \\
\Gamma_{abstr,Ru} &= \Gamma_{atom}\sigma_{abstr,Ru}n_{surf,Ru} \\
\Gamma_{desorp,RuO_2} &= 2k_{desorp}(2E_{desorp,RuO_2})n_{surf,RuO_2}^2 \\
\Gamma_{desorp,Ru} &= 2k_{desorp}(2E_{desorp,Ru})n_{surf,Ru}^2 \\
\Gamma_{absorp,Sn} &= k_{absorp}(E_{absorp,Sn})n_{surf,Sn} \\
\Gamma_{absorp,Ru} &= k_{absorp}(E_{absorp,Ru})n_{surf,Ru} \\
\Gamma_{resurf,Sn} &= k_{resurf}c_{sub,Sn}(\theta_{Sn} - \theta_{D,Sn}) \\
\Gamma_{resurf,Ru} &= k_{resurf}c_{sub,Ru}(\theta_{Ru} - \theta_{D,Ru}) \\
\Gamma_{diff,Sn} &= \frac{D_{diff,Ru}}{d_{Ru}}(c_{sub,Sn} - c_{bulk}) \\
\Gamma_{diff,Ru} &= \frac{D_{diff,Ru}}{d_{Ru}}(c_{sub,Ru} - c_{bulk}) \\
\Gamma_{trap} &= k_{trap}c_{bulk} \frac{c_{trap,max} - c_{trap}}{N_{latt,Ti}} \\
\Gamma_{detr} &= k_{detr}(c_{trap,max} - c_{trap})
\end{aligned} \tag{3}$$

where the parameters are divided into fixed parameters in Tab. 1 and Tab. 2, and free parameters in Tab. 3. Since the Ru-capped targets in this work are provided by the same supplier as that for our previous work [12], we use the parameters determined using our previous model as fixed parameters in this model as shown in Tab. 2. For the Sn-covered surface, we neglect the desorption process and assume a sticking coefficient of unity for deuterium atoms, since hydrogen radicals and Sn atoms lead to exothermic and spontaneous formation of stannane [35, 6]. By keeping all of the fixed parameters constant and varying the free ones, we fit the D retention with this model for all the exposure conditions in Fig. 6. As shown in Fig. 6(b), the model describes our experimental data reasonably well for the best-fit values of the free parameters in Tab. 3. In the next section, we will discuss possible mechanisms responsible for the drastic increase in the deuterium uptake based on the model. Moreover, we will also address the different trend of deuterium retention for more than one atomic layer of Sn as shown in Fig. 7, which is beyond the scope of the model.

fixed parameter	symbol	value	note
atom flux	Γ_{atom}	$2.3 \times 10^{22} \text{ m}^{-2} \text{ s}^{-1}$	experimental data
ion flux	Γ_{ion}	$4.2 \times 10^{19} \text{ m}^{-2} \text{ s}^{-1}$	experimental data
target temperature	T	23°C	experimental data
Ru layer thickness	d_{Ru}	40 nm	experimental data
Ti layer thickness	d_{Ti}	30 nm	experimental data
Ru lattice density	$N_{latt,Ru}$	$7.25 \times 10^{28} \text{ m}^{-3}$	experimental data
Ti lattice density	$N_{latt,Ti}$	$5.83 \times 10^{28} \text{ m}^{-3}$	experimental data
Ru lattice parameter	λ_{Ru}	$\sqrt[3]{N_{latt,Ru}}$	
Ti lattice parameter	λ_{Ti}	$\sqrt[3]{N_{latt,Ti}}$	
maximum surface coverage	n_{max}	λ_{Ru}^{-2}	defined as 1 ML
adsorbent surface coverage	θ_i	$\frac{n_i}{n_{max}}$	i = Ru, RuO ₂ , Sn
D surface coverage	$\theta_{D,i}$	$\frac{n_{surf,i}}{n_{max}}$	i = Ru, RuO ₂ , Sn
pre-exponential factor	ν_0	10^{13} Hz	[36, 37]
adsorption cross section	σ_{adsorp}	3.2 \AA^2	metallic Ru [38]
abstraction cross section	σ_{abstr}	1.1 \AA^2	metallic Ru [39]
Ru desorption barrier	$2E_{desorp,Ru}$	1.04 eV	metallic Ru [40]
detrapping barrier	E_{detr}	1.53 eV	[41]
maximum trapped concentration	$c_{trap,max}$	$\frac{n_{trap,max}}{d_{Ti}}$	$n_{trap,max} = 3.5 \times 10^{21} \text{ m}^{-2}$
diffusion coefficient for Ti	$D_{diff,Ti}$	$1.03 \times 10^{-14} \text{ m}^2/\text{s}$	[42]
escape rate constant	k_{es}	$\nu_0 \exp(-\frac{E_{es}}{k_B T})$	[36]
return rate constant	k_{re}	$\nu_0 \exp(-\frac{E_{re}}{k_B T})$	[36]
desorption rate constant	$k_{desorp}(2E_{desorp})$	$\nu_0 \lambda_{Ru}^2 \exp(-\frac{2E_{desorp}}{k_B T})$	[36, 43, 37]
absorption rate constant	$k_{absorp}(E_{absorp})$	$\nu_0 \exp(-\frac{E_{absorp}}{k_B T})$	[36, 43, 37]
resurfacing rate constant	k_{resurf}	$\nu_0 \lambda_{Ru} \exp(-\frac{E_{resurf}}{k_B T})$	[36, 43, 37]
trapping rate constant	k_{trap}	$\frac{D_{diff,Ti}}{\lambda_{Ti}}$	[37]
detrapping rate constant	k_{detr}	$\nu_0 \lambda_{Ti} \exp(-\frac{E_{detr}}{k_B T})$	[37]

Table 1: Fixed Parameters in the Reaction-Diffusion Model.

fixed parameter	symbol	value	note
oxide removal yield	ξ	2×10^{-3} for $E_{ion} = 1$ eV 1×10^{-2} for $E_{ion} = 20$ eV	Ion energy dependent [44, 12]
absorption barrier	$E_{absorp,Ru}$	0.87 eV	[10, 34]
resurfacing barrier	E_{resurf}	0.62 eV	[10, 34]
diffusion coefficient for Ru	$D_{dif,Ru}$	5.33×10^{-13} m ² /s	[33]

Table 2: Fixed Parameters in the Reaction-Diffusion Model, Determined in [12].

free parameter	symbol	best fit	note
escape barrier	E_{es}	0.44 eV	[45, 46]
return barrier	E_{re}	1.19 eV	[11]
RuO ₂ desorption barrier	$2E_{desorp,RuO_2}$	0.55 eV	[28]
Sn absorption barrier	$E_{absorp,Sn}$	0.73 eV	[10, 11]

Table 3: Free Parameters in the Reaction-Diffusion Model.

5 Discussion

5.1 Less than One Atomic Layer of As-Deposited Sn

The acceleration of the deuterium uptake induced by Sn, as shown in Fig. 6, is qualitatively consistent with the predictions based on DFT in [10, 11]. According to these studies, when a Sn atom or a Sn hydride molecule is adsorbed on the Ru(0001) surface, charge transfer from Sn to H and Ru reduces their atomic volumes, making hydrogen penetration more favorable. This also holds for a complete atomic layer of Sn on Ru because hydrogen can access the Ru lattice through the Sn layer, given the larger atom size of Sn than Ru. The presence of Sn on Ru increases the energy of hydrogen at the surface with respect to the subsurface and a significant drop in the absorption barrier. The hydrogen with Sn on Ru is 0.75 – 1.33 eV higher in energy than only Ru. The calculated absorption barrier is 1.06 eV for only hydrogen on Ru, and drops to 0.28 – 0.83 eV for SnH_x molecules (x=1, 2, 3, and 4) on Ru [10, 11]. In our model, the best-fit value of the absorption barrier is 0.73 eV for the Sn surface, which is reasonably close to the computed value for the SnH case (0.80 eV). We assume a constant absorption barrier with respect to the Sn content, since a DFT study shows that the energy barrier of hydrogen only slightly changes when the Sn content increases from 1/9 to 1/4 ML [47]. It is also worthwhile to note that [47] reports a negligible influence of the Sn content on the energy barrier of hydrogen, which is different than the results from [10, 11]. Further studies are needed to clarify this discrepancy before the influence of Sn that we observed can be applied to other systems.

Nonetheless, if we only consider depth-wise transport of deuterium through the layers, the drastic increase in the uptake rate cannot be quantitatively explained by the lower absorption barrier. As described in [12] and Sec. 4, our model indicates that the deuterium uptake is surface-limited, which means the uptake rate depends on the deuterium surface concentration and the absorption barrier. For less than 0.67 ML of Sn on Ru, the surface is covered by less than an atomic layer of Sn atoms; therefore, the Sn surface coverage (θ_{Sn}) increases linearly with the as-deposited Sn content. Assuming similar deuterium surface concentrations on Sn and Ru, the uptake rate for the Sn surface is expected to be much higher than Ru due to the Arrhenius relationship with the absorption barrier. If there is no interaction among RuO₂, Sn, and Ru surfaces, one would expect the uptake rate to linearly increase with θ_{Sn} , which is obviously not what we observe in the experiment. This discrepancy also shows the necessity of using our model to find out more relevant processes to the deuterium uptake.

To explain the nonlinear increase in the uptake rate, we propose lateral surface transport of deuterium in the model, including escape and return fluxes ($\Gamma_{es,j}$ and $\Gamma_{re,j}$). These fluxes in combination with the desorption flux from the RuO₂ surface act as a drain for deuterium on the Sn surface. As shown in Tab. 3, the determined E_{es} , E_{re} , and $2E_{desorp,RuO_2}$ are 0.44, 1.19, and 0.55 eV, respectively, while $2E_{desorp,Ru}$ is 1.04 eV. This indicates high escape fluxes from the Sn surface to the other surfaces and a high desorption flux on the

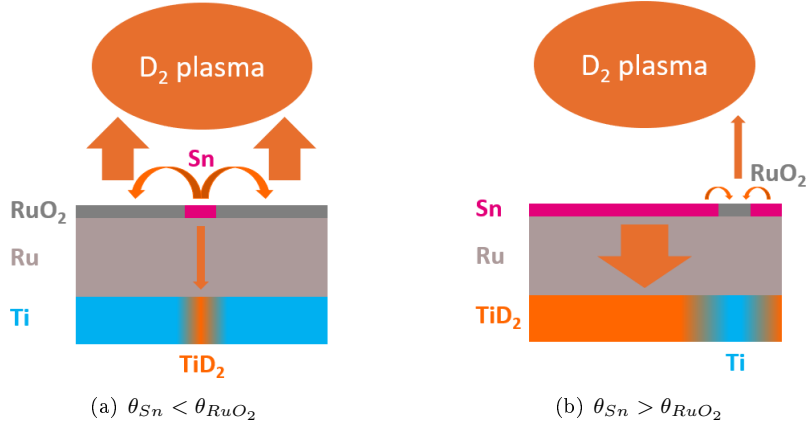


Figure 9: Illustration of the deuterium fluxes in the target during the plasma exposure for the as-deposited Sn content of less than one atomic layer. The arrows represent the deuterium fluxes and the width of the arrow refers to the magnitude of the flux. The arrows from the surface to the plasma and to the Ti layer represent the deuterium thermal desorption and implantation fluxes, respectively. Two cases are used to illustrate the strong dependence of the draining process and the deuterium uptake on the Sn surface coverage. (a) Sn surface coverage is less than the RuO_2 surface coverage, leading to a strong draining process and weak deuterium uptake. (b) Sn surface coverage is more than the RuO_2 surface coverage, leading to a weak draining process and strong deuterium uptake.

RuO_2 surface. When deuterium from the plasma sticks to the Sn surface, it can easily migrate to the RuO_2 or Ru surfaces via the escape process, and hardly returns to the Sn surface due to the high return barrier E_{re} . The migration can lead to a deuterium saturated Ru surface, which extinguishes the escape flux to Ru. On the other hand, deuterium migrating to the RuO_2 surface can leave the system via strong desorption Γ_{desorp, RuO_2} . The empty sites created on the RuO_2 surface can therefore accommodate the next deuterium atoms migrating from the Sn surface, which will be drained by another desorption process. Note that in this model we assume the deuterium migration from Ru to RuO_2 is negligible compared to that from Sn to RuO_2 because hydrogen tends to be energetically more stable at the Ru than Sn surface [11].

This series of processes significantly drains deuterium on the Sn surface for a high RuO_2 surface coverage (θ_{RuO_2}), leading to the nonlinear increase in the uptake rate. When θ_{Sn} is low ($\theta_{Sn} < \theta_{RuO_2}$), there can be more empty sites on the RuO_2 surface than the deuterium atoms occupying the Sn surface. In this case, the combination of the escape and desorption processes can effectively lower the deuterium surface coverage on the Sn surface ($\theta_{D, Sn}$), as illustrated in Fig. 9(a). However, when θ_{Sn} is high ($\theta_{Sn} > \theta_{RuO_2}$), there are not enough

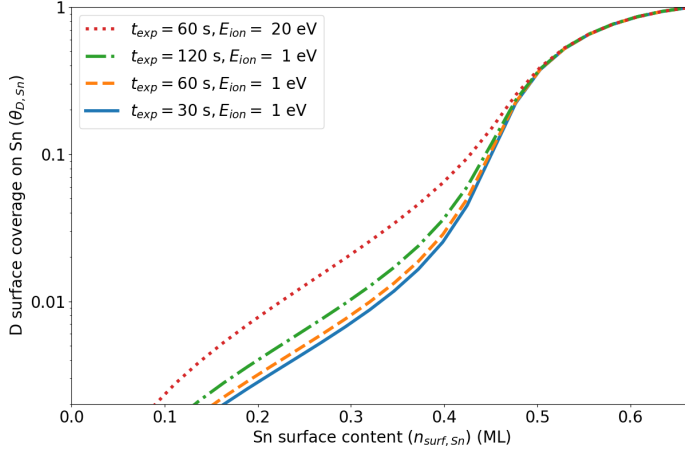


Figure 10: Calculated deuterium surface coverage on the Sn surface at the end of the deuterium plasma exposure. The calculation is performed using the model described in the text with the fixed parameters in Tab. 2 and Tab. 1, and the best-fit values of the free parameters in Tab. 3.

sites on the RuO_2 surface to accommodate the migrating deuterium from the Sn surface. Therefore $\theta_{D,Sn}$ increases drastically with θ_{Sn} . Once θ_{Sn} is close to unity, the draining process has little effect because there is hardly any RuO_2 surface for deuterium to escape to, as illustrated in Fig. 9(b). Overall, our calculation using the model indicates that $\theta_{D,Sn}$ increases nonlinearly with θ_{Sn} as shown in Fig. 10. This accounts for the nonlinear increase in the uptake rate, which is dominated by the absorption flux $\Gamma_{absorp,Sn}$ and therefore dependent on $\theta_{D,Sn}$.

The time evolution of the RuO_2 surface also has an influence on the uptake rate. As shown in Fig. 6(b), at an ion energy of 1 eV, the retention generally increases with the fluence due to the absorption processes. It is important to note that the escape flux to RuO_2 decreases with the fluence because θ_{RuO_2} drops during the Ru oxide removal. This results in an increase in $\theta_{D,Sn}$ and consequently an increase in the deuterium uptake rate. The effect of oxide removal also accounts for the higher uptake rate at an ion energy of 20 eV than 1 eV only for the low Sn surface coverage. As shown in Tab. 2, the oxide removal efficiency at 20 eV is 5 times that at 1 eV. When θ_{Sn} is low, there is initially a large RuO_2 surface, which becomes reduced very quickly at an ion energy of 20 eV, leading to a lower escape flux and a higher $\theta_{D,Sn}$ than with an ion energy of 1 eV. Therefore, the uptake rate is elevated at an ion energy of 20 eV compared with 1 eV. On the other hand, when θ_{Sn} is high, there is limited RuO_2 surface to be reduced by the plasma and the escape flux is low from the beginning of the exposure. Hence, the difference of $\theta_{D,Sn}$ between 20 and 1 eV is small, leading to the similar uptake rate. The calculated $\theta_{D,Sn}$ as a function of θ_{Sn} clearly

shows the influence of the ion energy on the interplay between $\theta_{D,Sn}$, θ_{Sn} , and θ_{RuO_2} as depicted in Fig. 10.

We also investigate the possible mechanisms related to the draining process based on the determined parameters E_{es} , E_{re} , and $2E_{desorp,RuO_2}$. To compare with results in the literature, we use $2E_{desorp,RuO_2}$ to estimate the peak temperature T_{peak} in thermal desorption spectroscopy (TDS) measurements. When the desorption flux Γ_{desorp,RuO_2} reaches its peak, the relation between T_{peak} and $2E_{desorp,RuO_2}$ is given by [48]

$$\frac{2E_{desorp,RuO_2}}{k_B T_{peak}^2} = \frac{\theta_{D,RuO_2,0} \nu_0}{\beta} \exp\left(\frac{-2E_{desorp,RuO_2}}{k_B T_{peak}}\right) \quad (4)$$

where $\theta_{D,RuO_2,0}$ and β refer to the initial deuterium surface coverage and the heating rate, respectively. Assuming $\theta_{D,RuO_2,0} = 0.5$ and $\beta = 1 \text{ K/s}$, the numerical solution of Eq. 4 for T_{peak} is 205 K, which is reasonably consistent with the peaks at 100 K and around 260 K in the TDS experiments in the literature [49, 28, 50]. Interestingly, these TDS studies suggest that the peak at 100 K results from deuterium desorption at coordinatively unsaturated Ru sites (Ru_{cus}) [50] while the broad feature around 260 K is related to defects such as Ru islands on the RuO_2 surface. [28]. This indicates that the preparation of the target surface could have a strong influence on the deuterium desorption from the RuO_2 surface and subsequently the draining process. Nevertheless, even starting with a clean RuO_2 surface, the target is expected to be fully reduced to Ru after long deuterium plasma exposure. Therefore we expect the draining process eventually ends due to lack of RuO_2 on the surface.

The escape and return barriers E_{es} and E_{re} are also determined by using our model. Here, we focus on the escape process that leads to deuterium migration from the Sn to RuO_2 surfaces, since it is an important part of the draining process. Unfortunately, the underlying theory has never been studied, so here we propose two possible mechanisms to account for this escape process. One mechanism is the spillover effect, as mentioned earlier. It has been shown that for the spillover effect, hydrogen diffusing from the metal catalyst to the support could leave the support via thermal desorption as hydrogen molecules [51, 52], which is consistent with the draining process in our model. As described in Sec. 4, the spillover effect is energetically possible since hydrogen on Sn has a higher energy than Ru by 0.75 – 1.33 eV based on DFT results. We expect it is also energetically favorable for deuterium to escape from the Sn to RuO_2 surfaces because deuterium on the RuO_2 surface is only higher than Ru by $E_{desorp,Ru} - E_{desorp,RuO_2} = 0.24 \text{ eV}$ in energy in our model. For the spillover effect to occur, DFT studies suggest that one needs dissociated hydrogen atoms on the metal catalyst and strong interactions between the metal and the support [2]. These two criteria could be applied to our model, since we have dissociated deuterium atoms available on Sn upon deuterium plasma exposure and strong atomic interactions between Sn and Ru based on DFT studies [10, 11]. The details of this proposed mechanism may still need to be verified by further computational studies.

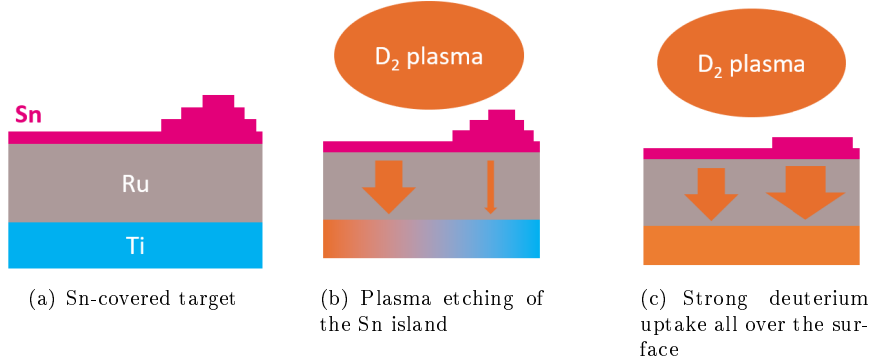


Figure 11: Schematics of the time evolution of the film stack during plasma exposure. The width of the arrow from the surface to the Ti layer represents the magnitude of the deuterium implantation flux. (a) Target surface is initially covered by an atomic layer of Sn and a 3D Sn island on the first atomic layer. (b) Upon plasma exposure, the deuterium uptake in Ru is accelerated by the atomic layer of Sn but hindered by the Sn island, on which Sn etching takes place during this period. (c) After the Sn island shrinks due to Sn etching, the deuterium uptake is accelerated all over the target surface.

The other possible mechanism for the escape process is decomposition of SnD_x ($x = 1, 2, 3,$ and 4) on Ru. As mentioned in Sec. 4, volatile species SnD_x could form near the target surface upon exposure to deuterium plasma. Due to strong interactions between Sn and Ru, SnH_4 can decompose into Sn and H on the Ru surface, as experimentally demonstrated in [6, 7, 46], effectively leading to H migration from Sn to Ru. However, we do not find the corresponding energy barrier to compare with $E_{es} = 0.44 \text{ eV}$ in our model, whereas 0.39 and 0.47 eV are reported in [45] and [46], respectively, for the energy barrier for SnH_4 decomposition on Sn. Furthermore, although DFT studies show that H released by SnH_x can penetrate into the Ru subsurface [10, 11], there is still lack of computational investigation of lateral H migration from SnH_x to RuO_2 or Ru on the surface. More computational studies are certainly required to validate this hypothesis.

5.2 More than One Atomic Layer of As-Deposited Sn

θ_{Sn} of unity is a turning point for both the Sn etching and deuterium uptake, based on comparison of the results shown in Fig. 6 and Fig. 7. As θ_{Sn} goes above unity, the model described in Sec. 4 cannot be applied, because DFT studies show that 3D Sn islands form on the first atomic layer of Sn on Ru [11], which contradicts with the first assumption of our model. In contrast to no Sn loss for $\theta_{\text{Sn}} < 1$, the Sn content clearly drops after the plasma exposure

for $\theta_{Sn} > 1$, which can be explained by Sn etching by forming volatile SnD_x upon exposure to hydrogen plasmas or radicals, as extensively investigated in [6, 27, 5]. However, all these studies were carried out for Sn layers with thickness of several tens to several hundreds of nanometers, which is much more than MLs in our experiments. To explain removal of the MLs of Sn, we speculate that the Sn etching is facilitated by weak SnD_x decomposition for $\theta_{Sn} > 1$ because SnD_x molecules cannot easily access the Ru surface which is already covered by a single layer of Sn. After the Sn etching, the residual Sn content is higher than that of the as-deposited Sn, which means the as-deposited Sn islands cannot be fully removed, even by increasing the exposure time from 30 to 60 s. This finding could be explained by formation of 3D Sn islands on the Ru surface upon hydrogen radical exposure in the presence of Sn as reported in [35]. The competition between removal and formation of the 3D Sn islands might determine the residual Sn content upon the plasma exposure. Note that the residual Sn content is always higher than one atomic layer because the first atomic layer of Sn cannot be removed due to strong SnD_x decomposition, as discussed in Sec. 4.

More importantly, the residual Sn content could help us to understand the trend of the deuterium retention. The Sn etching appears to occur only during the first 30 s or less because the plasma exposures for 30 and 60 s yield similar amounts of the residual Sn. The system reaches an equilibrium state within 30 s upon plasma exposure and the resulting amount of residual Sn increases with the as-deposited Sn content, as indicated by the dotted line in Fig. 7(a). This line corresponds to data fit with a linear function $0.43n_{Sn} + 0.39$, where n_{Sn} is the as-deposited Sn concentration at the surface in ML. Based on this linear fit, the calculated amount of the etched Sn is $n_{Sn} - (0.43n_{Sn} + 0.39) = 0.57n_{Sn} - 0.39$ ML, which linearly increases with n_{Sn} . If we assume the same etch rate for all n_{Sn} in the experiment, the time for etching also increases with n_{Sn} before the residual Sn reaches its minimum content at equilibrium. DFT studies show that hydrogen uptake is seriously suppressed for $\theta_{Sn} > 1$ compared with $\theta_{Sn} < 1$ [11], so we assume during the first 30 s, Sn etching first occurs on the 3D islands where the deuterium uptake is hindered. Intuitively, when deuterium is partially consumed by forming SnD_4 , a lower amount of deuterium can penetrate the Ru surface. However, this cannot fully explain the seriously hindered deuterium uptake as shown in Fig. 7(a). For the as-deposited Sn content of 1.5 ML, the first 30 s of plasma exposure yielded an etched Sn content of about 4.65×10^{18} atoms/m², which consumes only 1.86×10^{19} atoms/m² of deuterium while almost no Sn is etched for the as-deposited Sn content of 0.8 ML. On the other hand, as shown in Fig. 7(b), the deuterium retention for 1.5 ML of Sn is lower than that for 0.8 ML by 15% of the total traps, which corresponds to 5.25×10^{20} atoms/m² of deuterium. This suggests that a small amount of deuterium consumption on the surface can lead to more than 10 times more loss of the deuterium retention. Therefore we conclude that Sn islands not only consume deuterium but also slow down the deuterium penetration through the underlying Sn and the Ru surface.

When the Sn island concentration reaches the equilibrium, the deuterium uptake rate goes up in the presence of the residual Sn as depicted in Fig. 11.

Therefore, since the etching time increases with n_{Sn} , the time for the deuterium uptake decreases with n_{Sn} , leading to the decreasing trend of the deuterium retention after exposures for 30 s. Furthermore, as we increase the exposure time from 30 to 60 s, the deuterium retention becomes similar for all n_{Sn} in Fig. 7. Since the system already reaches the equilibrium during this period, we assume no Sn etching and only deuterium uptake in the presence of Sn. This means the deuterium uptake rate from 30 to 60 s could increase with n_{Sn} and compensate for the delayed deuterium uptake due to Sn etching during the first 30 s. Combining our results for $\theta_{Sn} < 1$ and $\theta_{Sn} > 1$, we hypothesize that when the Sn etching is hindered, the deuterium uptake rate always increases with n_{Sn} up to a few MLs of the residual Sn. However, the interplay between Sn etching and hydrogen uptake in Ru in the presence of Sn still needs to be further investigated with support of computational studies to validate our hypotheses.

6 Conclusions

We present the first experimental demonstration of the promoted deuterium uptake in Ru films in the presence of Sn upon plasma exposure. For the deposited Sn of less than one atomic layer, no Sn removal occurs, and the deuterium uptake rate increases nonlinearly with the Sn content by 2–3 orders of magnitude. This result is consistent with the low hydrogen absorption barrier induced by a single layer of Sn as reported in recent DFT studies. Furthermore, we successfully simulate the deuterium uptake using a reaction-diffusion model, including multiple surface species and relevant processes. This model shows the importance of the proposed draining process, which requires deuterium lateral migration from the Sn to RuO₂ surfaces and strong deuterium desorption from the RuO₂ surface. Possible mechanisms, such as the spillover effect, are proposed to account for the deuterium lateral migration. On the other hand, Sn removal starts to occur and the measured deuterium retention behaves differently when the as-deposited Sn content exceeds one atomic layer. Based on the residual Sn content and the deuterium retention, we hypothesize that upon plasma exposure, the deuterium uptake is first partially suppressed during the Sn removal, after which the deuterium uptake rate increases with the as-deposited Sn content in the ML range. This study is possibly helpful for understanding the interactions between Sn, Ru, and hydrogen in relation to the hydrogen uptake. More studies are still needed in order to develop a potential mitigation strategy for the blistering of Ru films in the presence of Sn.

7 Acknowledgment

This research was carried out under project number T16010b in the framework of the Research Program of the Materials innovation institute (M2i) (<https://www.m2i.nl>) supported by the Dutch government. This work has been carried out within the framework of the EUROfusion Consortium, funded by the European Union

via the Euratom Research and Training Programme (Grant Agreement No 101052200 - EUROfusion). Views and opinions expressed are however those of the author(s) only and do not necessarily reflect those of the European Union or the European Commission. Neither the European Union nor the European Commission can be held responsible for them. The authors would like to acknowledge ASML for their financial and technical support. We would like to thank Michel Riepen and Marise Gielen at ASML for the experiments on Diablo. We appreciate great help from Richard Al and Peter Wortman at DIFFER for designing and manufacturing components of nano-PSI. We also thank Wim Arnold Bik at DIFFER for fruitful discussion.

References

- [1] Zacharia, R., ullah Rather, S., Hwang, S. W., and Nahm, K. S. Spillover of Physisorbed Hydrogen from Sputter-deposited Arrays of Platinum Nanoparticles to Multi-walled Carbon Nanotubes. *Chemical Physics Letters*, 434(4):286–291, 2007.
- [2] Shen, H., Li, H., Yang, Z., and Li, C. Magic of Hydrogen Spillover: Understanding and Application. *Green Energy and Environment*, 7:1161, 2022.
- [3] Dumand, A., Minissale, M., Faure, J.-B., Gallais, L., Angot, T., and Bisson, R. Surface Oxygen versus Native Oxide on Tungsten: Contrasting Effects on Deuterium Retention and Release. *Nuclear Fusion*, 62(5):054002, Mar 2022.
- [4] van Herpen, M., Klunder, D., Soer, W., Moors, R., and Banine, V. Sn Etching with Hydrogen Radicals to Clean EUV Optics. *Chemical Physics Letters*, 484(4):197 – 199, 2010.
- [5] Ji, M., Nagata, R., and Uchino, K. Effect of Hydrogen Ion Energy in the Process of Reactive Ion Etching of Sn Thin Films by Hydrogen Plasmas. *Plasma and Fusion Research*, 16:1406003–1406003, 2021.
- [6] Ugur, D., Storm, A., Verberk, R., Brouwer, J., and Sloof, W. Decomposition of SnH₄ Molecules on Metal and Metal-oxide Surfaces. *Applied Surface Science*, 288:673 – 676, 2014.
- [7] Pachecka, M., Sturm, J. M., van de Kruijs, R. W. E., Lee, C. J., and Bijkerk, F. Electronegativity-dependent Tin Etching from Thin Films. *AIP Advances*, 6(7):075222, 2016.
- [8] Kuznetsov, A. S., Gleeson, M. A., and Bijkerk, F. Hydrogen-induced Blistering Mechanisms in Thin Film Coatings. *Journal of Physics: Condensed Matter*, 24(5):052203, Dec 2011.

- [9] Tomuro, H., Ji, M., Nagata, R., Kouge, K., Yanagida, T., Morita, M., Andou, M., Honda, Y., Uchino, K., and Yoshitake, T. Evaluation of Hydrogen-Induced Blistering of Mo/Si Multilayers with a Capping Layer. *Plasma and Fusion Research*, 17(1406005), 2022.
- [10] Onwudinanti, C., Tranca, I., Morgan, T., and Tao, S. Tin, the Enabler - Hydrogen Diffusion into Ruthenium. *Nanomaterials*, 9(129), January 2019.
- [11] Onwudinanti, C., Brocks, G., Koelman, V., Morgan, T., and Tao, S. Tin Deposition on Ruthenium and its Influence on Blistering in Multi-layer Mirrors. *Phys. Chem. Chem. Phys.*, 23:13878–13884, 2021.
- [12] Wang, S. C., Zoethout, E., van Kampen, M., and Morgan, T. W. Surface-limited Deuterium Uptake of Ru Films under Plasma Exposure. *Journal of Applied Physics*, 132(22):225903, 2022.
- [13] Paffett, M. T., Logan, A. D., and Taylor, T. N. Tin Deposition on Ruthenium (001): a Multitechnique Surface Science Study. *The Journal of Physical Chemistry*, 97(3):690–695, 1993.
- [14] Yuhara, J., Ishikawa, Y., and Matsui, T. Two-dimensional Alloy of Immiscible Pb and Sn Atoms on Ru(0001). *Surface Science*, 616:131–136, 2013.
- [15] Topolnicki, R. and Kucharczyk, R. Structural and electronic properties of submonolayer-thick Sn films on Ru(0001). *Applied Surface Science*, 329:376–383, 2015.
- [16] Wang, S. C., van der Horst, R. M., van Kampen, M., and Morgan, T. W. Application of a Dual-thermopile Radical Probe to Expanding Hydrogen Plasmas. *Plasma Sources Science and Technology*, 31(8):085011, Aug 2022.
- [17] Bystrov, K., Morgan, T. W., Tanyeli, I., Temmerman, G. D., and van de Sanden, M. C. M. Chemical Sputtering of Graphite by Low Temperature Nitrogen Plasmas at Various Substrate Temperatures and Ion Flux Densities. *Journal of Applied Physics*, 114(13):133301, 2013.
- [18] Mazouffre, S. *Transport Phenomena in Plasma Expansions Containing Hydrogen : a Laser Spectroscopic Study*. PhD thesis, Department of Applied Physics, Eindhoven University of Technology, 2001. <https://doi.org/10.6100/IR547907>.
- [19] Vankan, P. *Molecules and Atoms in a Hydrogen Plasma Expansion*. PhD thesis, Department of Applied Physics, Eindhoven University of Technology, 2005. <https://doi.org/10.6100/IR583043>.
- [20] Bik, W. M. A. and Habraken, F. H. P. M. Elastic Recoil Detection. *Reports on Progress in Physics*, 56(7):859–902, Jul 1993.

- [21] Melngailis, J. Focused Ion Beam Induced Deposition: a Review. In Peckerar, M. C., editor, *Electron-Beam, X-Ray, and Ion-Beam Submicrometer Lithographies for Manufacturing*, volume 1465, pages 36 – 49. International Society for Optics and Photonics, SPIE, 1991.
- [22] Mund, B. K., Soroka, O., Sturm, J. M., van den Beld, W. T. E., Lee, C. J., and Bijkerk, F. Atomic H Diffusion and C Etching in Multilayer Graphene Monitored using a Y Based Optical Sensor. *Journal of Vacuum Science & Technology B*, 37(5):051801, 2019.
- [23] Mayer, M. SIMNRA User’s Guide version 7.03, 2020. <https://mam.home.ipp.mpg.de>.
- [24] Burrell, M. C. and Armstrong, N. R. Deuterium Uptake in Titanium Thin Films: the Effect of Oxide, and the Metal (Ti and Fe) Overlayers. *Surface Science*, 160(1):235–252, 1985.
- [25] Braginsky, O. V., Kovalev, A. S., Lopaev, D. V., Malykhin, E. M., Rakhimova, T. V., Rakhimov, A. T., Vasilieva, A. N., Zyryanov, S. M., Koshelev, K. N., Krivtsun, V. M., van Kampen, M., and Glushkov, D. Removal of Amorphous C and Sn on Mo:Si Multilayer Mirror Surface in Hydrogen Plasma and Afterglow. *Journal of Applied Physics*, 111(9):093304, 2012.
- [26] Elg, D. T., Sporre, J. R., Panici, G. A., Srivastava, S. N., and Ruzic, D. N. In situ Collector Cleaning and Extreme Ultraviolet Reflectivity Restoration by Hydrogen Plasma for Extreme Ultraviolet Sources. *Journal of Vacuum Science & Technology A*, 34(2):021305, 2016.
- [27] Elg, D. T., Panici, G. A., Liu, S., Girolami, G., Srivastava, S. N., and Ruzic, D. N. Removal of Tin from Extreme Ultraviolet Collector Optics by In-Situ Hydrogen Plasma Etching. *Plasma Chemistry and Plasma Processing*, 38(1):223–245, Jan 2018.
- [28] Knapp, M., Crihan, D., Seitsonen, A. P., Lundgren, E., Resta, A., Andersen, J. N., and Over, H. Complex Interaction of Hydrogen with the RuO₂(110) Surface. *The Journal of Physical Chemistry C*, 111(14):5363–5373, 2007.
- [29] Wallinga, J., Arnoldbik, W. M., Vredenberg, A. M., Schropp, R. E. I., and van der Weg, W. F. Reduction of Tin Oxide by Hydrogen Radicals. *The Journal of Physical Chemistry B*, 102(32):6219–6224, 1998.
- [30] Thomas III, J. H. X-ray Photoelectron Spectroscopy Study of Hydrogen Plasma Interactions with a Tin Oxide Surface. *Applied Physics Letters*, 42(9):794–796, 1983.
- [31] Jadon, A., Rossi, C., Djafari-Rouhani, M., Estève, A., and Pech, D. Interaction of Hydrogen with the Bulk, Surface and Subsurface of Crystalline RuO₂ from First Principles. *Physics Open*, 7:100059, 2021.

- [32] Mak, C., Brand, J., Koehler, B., and George, S. Isotope Effect in the Surface Diffusion of Hydrogen and Deuterium on Ru(001). *Surface Science*, 188(1):312–320, 1987.
- [33] Onwudinanti, C., Pols, M., Brocks, G., Koelman, V., van Duin, A. C. T., Morgan, T., and Tao, S. A ReaxFF Molecular Dynamics Study of Hydrogen Diffusion in Ruthenium - The Role of Grain Boundaries. *The Journal of Physical Chemistry C*, 126(13):5950–5959, 2022.
- [34] Onwudinanti, C., Brocks, G., Koelman, V., Morgan, T., and Tao, S. Hydrogen Diffusion out of Ruthenium - an ab initio Study of the Role of Adsorbates. *Phys. Chem. Chem. Phys.*, 22:7935–7941, 2020.
- [35] Faradzhev, N. and Sidorkin, V. Hydrogen Mediated Transport of Sn to Ru Film Surface. *Journal of Vacuum Science & Technology A: Vacuum, Surfaces, and Films*, 27(2):306–314, 2009.
- [36] Pick, M. and Sonnenberg, K. A Model for Atomic Hydrogen-Metal Interactions – Application to Recycling, Recombination and Permeation. *Journal of Nuclear Materials*, 131(2):208 – 220, 1985.
- [37] Hodille, E., Založnik, A., Markelj, S., Schwarz-Selinger, T., Becquart, C., Bisson, R., and Grisolia, C. Simulations of Atomic Deuterium Exposure in Self-damaged Tungsten. *Nuclear Fusion*, 57(5):056002, Mar 2017.
- [38] Jachimowski, T. A. and Weinberg, W. H. Direct Reaction of Gas-phase Atomic Hydrogen with Chemisorbed Hydrogen on Ru(001). *The Journal of Chemical Physics*, 101(12):10997–11003, 1994.
- [39] Weiss, M. J., Hagedorn, C. J., and Weinberg, W. Interaction of Microwave Discharge-produced Atomic Hydrogen with Ru(001). *Surface Science*, 429(1):54–62, 1999.
- [40] Jachimowski, T. A., Meng, B., Johnson, D. F., and Weinberg, W. H. Thermal Desorption Studies of High-coverage Hydrogen Overlayers on Ru(001) Created with Gas-phase Atomic Hydrogen. *Journal of Vacuum Science & Technology A*, 13(3):1564–1568, 1995.
- [41] Checchetto, R., Gratton, L. M., Miotello, A., Tomasi, A., and Scardi, P. Structural Evolution and Thermal Stability of Deuterated Titanium Thin Films. *Phys. Rev. B*, 58:4130–4137, Aug 1998.
- [42] Miyoshi, T., Naito, S., Yamamoto, M., Doi, M., and Kimura, M. Diffusion of Hydrogen in Titanium, Ti88Al12 and Ti3Al. *J. Chem. Soc., Faraday Trans.*, 92:483–486, 1996.
- [43] Ogorodnikova, O. Comparison of Hydrogen Gas-, Atom- and Ion-metal Interactions. *Journal of Nuclear Materials*, 277(2):130 – 142, 2000.

- [44] Dolgov, A., Lee, C. J., Bijkerk, F., Abrikosov, A., Krivtsun, V. M., Lopaev, D., Yakushev, O., and van Kampen, M. Plasma-assisted Oxide Removal from Ruthenium-coated EUV Optics. *Journal of Applied Physics*, 123(15):153301, 2018.
- [45] Tamaru, K. The Thermal Decomposition of Tin Hydride. *The Journal of Physical Chemistry*, 60(5):610–612, 1956.
- [46] Panici, G. A., Qerimi, D., and Ruzic, D. N. Study of Sn Removal by Surface Wave Plasma for Source Cleaning (Conference Presentation). In Goldberg, K. A., editor, *Extreme Ultraviolet (EUV) Lithography IX*, volume 10583. International Society for Optics and Photonics, SPIE, 2018.
- [47] Gebhardt, J. and Urban, D. F. Influence of Impurity Atoms on Hydrogen Diffusion into Ruthenium. *The Journal of Physical Chemistry C*, 126(46):19895–19903, 2022.
- [48] Redhead, P. Thermal Desorption of Gases. *Vacuum*, 12(4):203–211, 1962.
- [49] Wang, J., Fan, C. Y., Sun, Q., Reuter, K., Jacobi, K., Scheffler, M., and Ertl, G. Surface Coordination Chemistry: Dihydrogen versus Hydride Complexes on RuO₂(110). *Angewandte Chemie International Edition*, 42(19):2151–2154, 2003.
- [50] Henderson, M. A., Dahal, A., Dohnálek, Z., and Lyubinetsky, I. Strong Temperature Dependence in the Reactivity of H₂ on RuO₂(110). *The Journal of Physical Chemistry Letters*, 7(15):2967–2970, 2016. PMID: 27434420.
- [51] Karim, W., Spreafico, C., Kleibert, A., Gobrecht, J., VandeVondele, J., Ekinci, Y., and van Bokhoven, J. A. Catalyst Support Effects on Hydrogen Spillover. *Nature*, 541(7635):68–71, Jan 2017.
- [52] Spreafico, C., Karim, W., Ekinci, Y., van Bokhoven, J. A., and VandeVondele, J. Hydrogen Adsorption on Nanosized Platinum and Dynamics of Spillover onto Alumina and Titania. *The Journal of Physical Chemistry C*, 121(33):17862–17872, 2017.